Development of a Flexible Turbine Cooling Prediction Tool for Preliminary Design of Gas Turbines

Yin, Feijia; Tiemstra, Floris S.; Gangoli Rao, Arvind

DOI
10.1115/1.4039732

Publication date
2018

Document Version
Final published version

Published in
Journal of Engineering for Gas Turbines and Power

Citation (APA)
Yin, F., Tiemstra, F. S., & Gangoli Rao, A. (2018). Development of a Flexible Turbine Cooling Prediction Tool for Preliminary Design of Gas Turbines. *Journal of Engineering for Gas Turbines and Power*, *140*(9), 091201-1 - 091201-12. Article GTP-18-1043. https://doi.org/10.1115/1.4039732

Feijia Yin
Faculty of Aerospace Engineering,
Delft University of Technology,
Kluyverweg 1,
Delft 2629 HS, The Netherlands
e-mail: F.yin@tudelft.nl

Floris S. Tiemstra
Faculty of Aerospace Engineering,
Delft University of Technology,
Kluyverweg 1,
Delft 2629HS, The Netherlands
e-mail: Floris.tiemstra@gmail.com

Arvind G. Rao[1]
Faculty of Aerospace Engineering,
Delft University of Technology,
Kluyverweg 1,
Delft 2629 HS, The Netherlands
e-mail: A.gangolirao@tudelft.nl

Development of a Flexible Turbine Cooling Prediction Tool for Preliminary Design of Gas Turbines

As the overall pressure ratio (OPR) and turbine inlet temperature (TIT) of modern gas turbines are constantly being increased in the pursuit of increasing efficiency and specific power, the effect of bleed cooling air on the engine performance is increasingly becoming important. During the thermodynamic cycle analysis and optimization phase, the cooling bleed air requirement is either neglected or is modeled by simplified correlations, which can lead to erroneous results. In this current research, a physics-based turbine cooling prediction model, based on semi-empirical correlations for heat transfer and pressure drop, is developed and verified with turbine cooling data available in the open literature. Based on the validated model, a parametric analysis is performed to understand the variation of turbine cooling requirement with variation in TIT and OPR of future advanced engine cycles. It is found that the existing method of calculating turbine cooling air mass flow with simplified correlation underpredicts the amount of turbine cooling air for higher OPR and TIT, thus overpredicting the estimated engine efficiency.
[DOI: 10.1115/1.4039732]

1 Introduction

The development of the turbine cooling technology has been one of the main pillars in the development of gas turbine engines. As engine manufacturers are constantly pushing the design limits by constantly increasing the overall pressure ratio (OPR) and turbine inlet temperature (TIT), in the pursuit of increasing engine efficiency and specific power, the role of turbine cooling technology is gaining importance. This is despite the progress in the maximum allowable metal operating temperature (AMOT) due to advancements in turbine materials.

The turbine cooling system has evolved substantially over the years. It has enabled the turbine to operate at a significantly higher temperature than its maximum AMOT, as shown in Fig. 1. With the modern gas turbine engines pushing the TIT and OPR further, the turbine cooling air requirement increases nonlinearly. Such nonlinear characteristics can cause large uncertainties in predicting the actual cooling air requirement if a linear approximation is used. As a result, significant discrepancies would be obtained in calculating the cycle performance. Therefore, there is a need for a tool to predict the cooling air requirements during the preliminary design stage of an engine.

The engine manufacturers have a detailed cooling air prediction tool based on physics, their design knowledge, and experience. Such a tool is proprietary and is not available for scientific research. This work attempts to fill in this gap by providing a methodology of a physics-based one-dimensional tool, utilizing validated heat transfer correlations available in the open literature. This paper provides the reader with the findings of detailed thermal performance related study into the preliminary modeling possibilities of turbine cooling systems. In the first step, the modeling philosophies of various internal and external turbine-cooling components are elaborated followed by the model validation. Subsequently, the modular cooling system is combined with a gas turbine performance model to evaluate the effects of the turbine cooling system on the performance of an aero engine.

2 Overview of the Turbine Cooling Model

The turbine cooling model is a module-based simulation tool consisting of cooling techniques, which are typically used in modern gas turbine blades or vanes, for instance, external film cooling, internal rib turbulated cooling, internal pin-fin cooling, and jet impingement cooling. Each of these cooling techniques is developed as a separate subroutine. Depending on the specific geometry of a vane or blade, the corresponding subroutines are activated. A general flowchart indicating the order of executing these various submodules is presented in Fig. 2.

The turbine cooling model calculates the mass flow rate of cooling air ($\dot{m}_c$) required to cool the outer wall of a single turbine vane/blade for a given maximum allowable material temperature (T_{max}). The exit temperature of the coolant (T_{ac}), the exit pressure of the coolant (p_{ac}), and the amount of heat absorbed by the coolant (Q_{abs}) are additional output parameters of this tool. To start

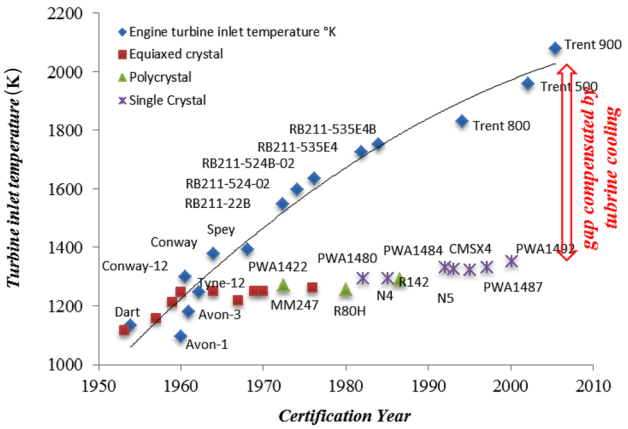

Fig. 1 Comparison of TIT and metal operating temperature [1]

[1]Corresponding author.

Contributed by the Aircraft Engine Committee of ASME for publication in the Journal of Engineering for Gas Turbines and Power. Manuscript received February 2, 2018; final manuscript received February 18, 2018; published online May 29, 2018. Editor: David Wisler.

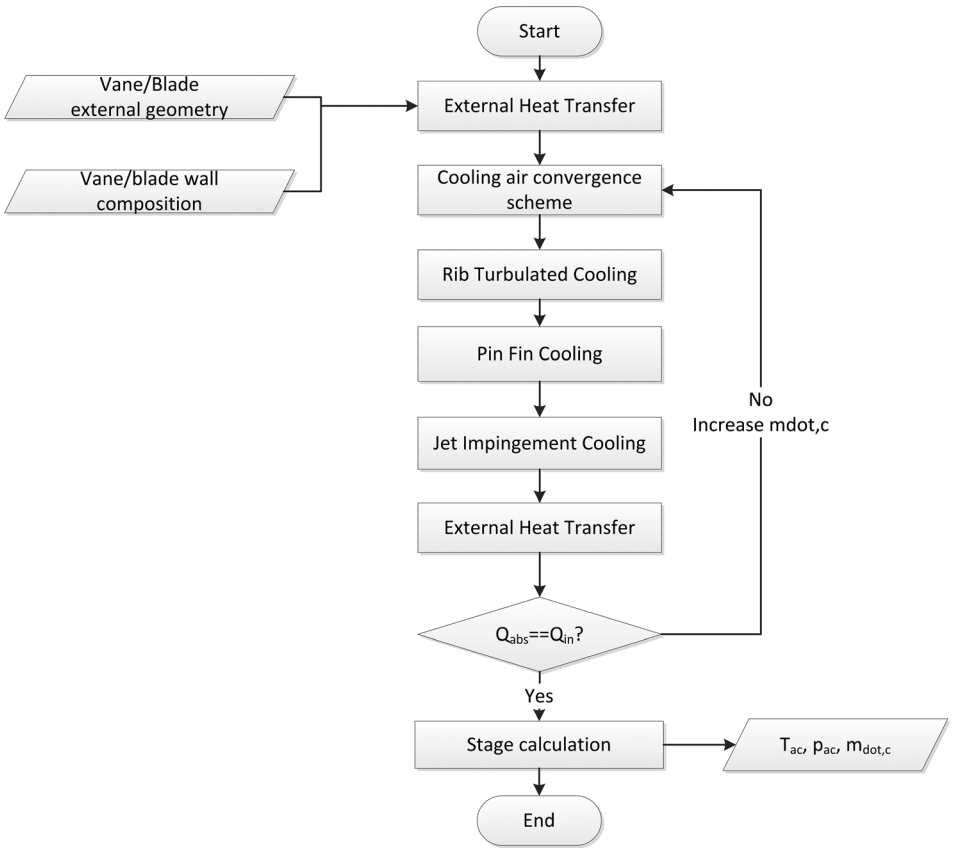

Fig. 2 Flowchart of the turbine cooling model

the model, information of the vane or blade geometry is required. The calculation procedure begins with the external heat transfer (film cooling) module followed by internal heat transfer modules including rib turbulated cooling, pin-fin cooling, and jet impingement cooling. The heat going into the blade (Q_{in}) and the heat absorbed (Q_{abs}) by a certain amount of cooling air are estimated. A convergence scheme is applied such that the heat flux between the external cooling and internal cooling ($Q = |Q_{in} - Q_{abs}|$) is balanced within a certain predefined error. Detailed information about the cooling convergence scheme will be discussed later in this section.

Moreover, as mentioned, a turbine geometry data would be required to initiate the model. At the conceptual analysis phase, the geometry of the turbine blade has not been finalized; therefore, the detailed information regarding the cooling arrangements is not available. A typical profile of a modern cooled turbine blade as presented in Fig. 3 is considered. It can be seen that at the leading edge of the blade, the jet impingement cooling approach is applied, followed by the downstream convection cooling within channels. The ribs and pin fins are used at different locations in the channels to improve the heat transfer rate. Depending on the arrangements of ribs and fins, the performance varies. The cooling flow spent from the leading edge by the jet impingement forms a film layer outside the blade surface to protect the blade from the hot gas. Each of the cooling mechanisms is elaborated in the following paragraphs.

3 Modeling Approach

3.1 External Heat Transfer. The amount of cooling air required is dependent on the heat that needs to be absorbed by the coolant. This heat flux should be equal to the heat going into the vane/blade to satisfy the physical laws for conservation of energy. This section will cover the determination of the external heat transfer into the vanes/blades. The distinction is made between the calculation of external heat transfer for film cooled and non-film cooled vanes/blades. For both, the first step is the determination of the velocity over the vane/blade (V) using the flow angles.

3.1.1 Nonfilm Cooled. For nonfilm-cooled vanes or blades, the Prandtl number Pr and Reynolds number Re follow from substitution of the gas properties, e.g., $c_{p\infty}$, μ_∞, k_∞ in Eqs. (1) and (2), respectively. The subscript ∞ indicates the free stream condition.

$$\mathrm{Pr} = \frac{c_{p\infty}\mu_\infty}{k_\infty} \tag{1}$$

$$\mathrm{Re} = \frac{\rho_\infty \cdot V \cdot C}{\mu_\infty} \tag{2}$$

From the Prandtl number Pr, a recovery factor r can be calculated. The Reynolds number Re at the wall determines the flow conditions (i.e., laminar, transient, or turbulent). Two situations are distinguished; for $\mathrm{Re} < 5 \times 10^5$, the flow is assumed to be laminar, and for $\mathrm{Re} > 5 \times 10^5$, the flow is assumed to be turbulent. The recovery factor is calculated for laminar and turbulent flow using Eqs. (3) and (4), respectively,

$$r = \sqrt{\mathrm{Pr}} \tag{3}$$

$$r = \sqrt[3]{\mathrm{Pr}} \tag{4}$$

Then, the adiabatic wall temperature (T_{aw}) can be calculated with the following equation, where T_s is the static temperature

$$T_{aw} = T_s + r\frac{V^2}{2\rho_\infty \cdot c_p} \tag{5}$$

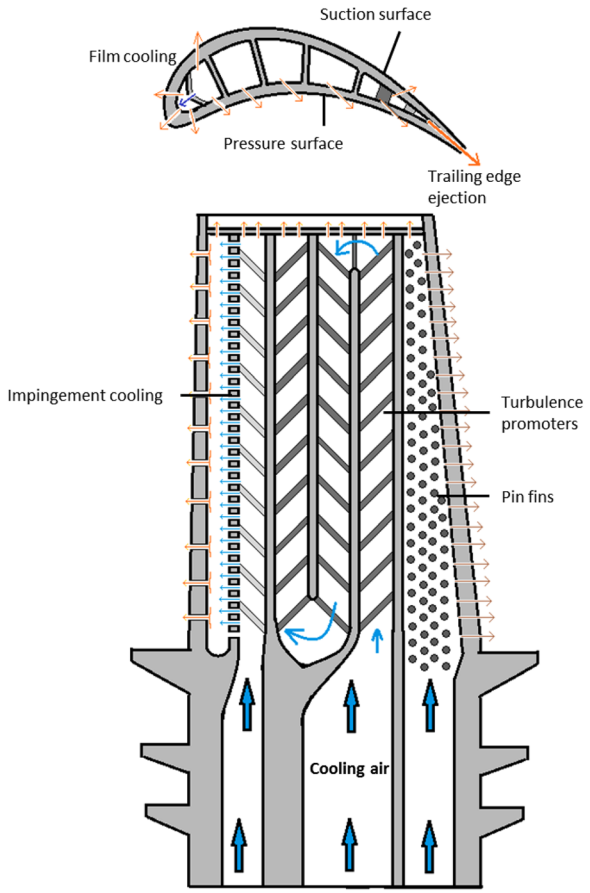

Fig. 3 Schematic of an advanced aero engine cooled HPT blade

3.1.2 Film Cooled. In the case that film cooling is applied, the film temperature T_f can be calculated by rewriting the equation for the film cooling effectiveness η_{film} as defined in the equation given below:

$$\eta_{\text{film}} = \frac{T_g - T_{\text{aw}}}{T_g - T_c} \tag{6}$$

In the turbine cooling tool, the film cooling effectiveness η_{film} is calculated by following the calculation scheme and the correlation outlined in Ref. [2], where the η_{film} is assumed to vary in the streamwise direction and is hence a function of the streamwise distance from the row of film cooling holes (x/D). Furthermore, η_{film} is dependent on the geometrical parameters such as the spanwise hole spacing (s/D_f), the injection angle (α_i), as well as the flow parameters like the mainstream turbulence intensity (T_u), the density ratio (DR), velocity ratio (VR), and blowing ratio (M).

For simplicity, the spanwise variation in film effectiveness is neglected by laterally averaging the film cooling effectiveness. The correlation for the averaged film cooling effectiveness $(\overline{\eta}_{\text{film}})$ has been taken from Ref. [2], and is given in the below equation:

$$\overline{\eta}_{\text{film}} = \eta_c \frac{\text{DR}^{0.09/s/D_f}}{(\sin\alpha_i)^{0.06 \cdot s/D_f}} \tag{7}$$

In this equation, the parameter η_c follows from an extensive series of calculations. More details can be found in Ref. [2], where a complete derivation of the determination of η_c are discussed.

With the $\overline{\eta}_{\text{film}}$ known, the film flow temperature can be calculated using the following equation:

$$T_f = T_g - \overline{\eta}_{\text{film}}(T_g - T_c) \tag{8}$$

The Prandtl number Pr and Reynolds number Re can now be calculated using Eqs. (1) and (2), respectively.

3.1.3 External Heat Transfer. For the determination of the external heat transfer coefficient h_o, the local Nusselt number $\text{Nu}(x)$ at the downstream location (x) is calculated. Depending on the flow regime, Eq. (9) is used to calculate the Nusselt number in laminar flow, and Eq. (10) is for turbulent flow

$$\text{Nu}(x) = 0.331\,\text{Pr}^{1/3} \tag{9}$$

$$\text{Nu}(x) = 0.0288\,\text{Pr}^{1/3}\,\text{Re}(x)^{4/5} \tag{10}$$

The local Nusselt number can be averaged to find the average Nusselt number (Nu). Together with the chord length (c_{vb}), the average Nusselt number over the external surface can be used in Eq. (11) to calculate the external surface heat transfer coefficient, h_o

$$h_o = \frac{k_\infty \cdot \text{Nu}}{c_{vb}} \tag{11}$$

Finally, the heat flux going into the vane/blade (Q_{in}) can be determined using Eq. (12), where A_{vb} is the external surface area of the vane/blade, h_o is the external surface heat transfer coefficient, and T_{max} is the maximum allowable metal temperature. T is equal to either the adiabatic wall temperature T_{aw} for the nonfilm cooled vanes/blades or to the film temperature T_f for the film cooled vanes/blades

$$Q_{\text{in}} = h_o A_{\text{vb}} \Delta T = h_o A_{\text{vb}}(T - T_{\text{max}}) \tag{12}$$

3.2 Internal Heat Transfer. For the internal cooling of the turbine vanes/blades, internal convection cooling channels with turbulence promoters are placed inside the vanes/blades. In the following paragraphs, the heat transfer mechanisms of the internal cooling techniques are described.

3.2.1 Rib Turbulated Cooling. This is the most widely used form of internal cooling technique in turbine blades and vanes. Ribs are turbulence promoters used in internal cooling channels. They cause a continuous detachment and re-attachment of the flow, thus promoting heat removal from the target surface, at the expenses of the total pressure.

The parameters, which influence the heat transfer performance of ribbed cooling channels, are the channel aspect ratio $(W_{\text{cc}}/H_{\text{o}})$ or AR, the rib height over hydraulic diameter (e/D_h), the rib spacing over rib height (P/e), the rib angle (α), the continuity of the ribs (i.e., continuous or discrete), and the rib shape (i.e., straight or V-shaped). A schematic of a channel with V-shaped ribs is depicted in Fig. 4. A selection process has been implemented in the current tool to flexibly configure the ribbed channels, as indicated in Fig. 5, which will yield different thermal performance characteristics.

For all rib configurations, the first few steps are identical. The channel height H_{cc} and width W_{cc} determine the cross-sectional area A_{cc} according to Eq. (13), and the hydraulic diameter of the channel D_h is then calculated following Eq. (14)

$$A_{\text{cc}} = H_{\text{cc}} W_{\text{cc}} \tag{13}$$

$$D_h = \frac{4W_{\text{cc}}H_{\text{cc}}}{2(W_{\text{cc}} + H_{\text{cc}})} = \frac{4A_{\text{cc}}}{P_{\text{cc}}} \tag{14}$$

With the A_{cc} known and substituting the cooling air mass flow rate $\dot{m}_c$ and the density of the coolant ρ_c, the flow velocity inside

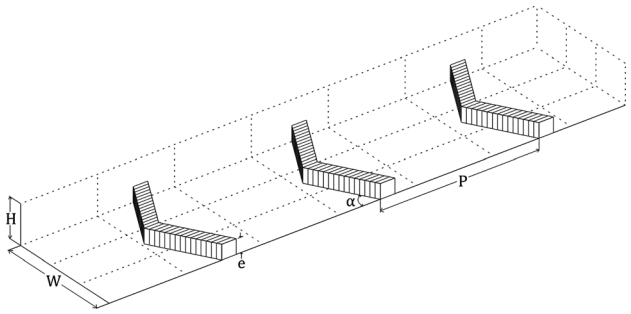

Fig. 4 Schematic of a channel with ribs

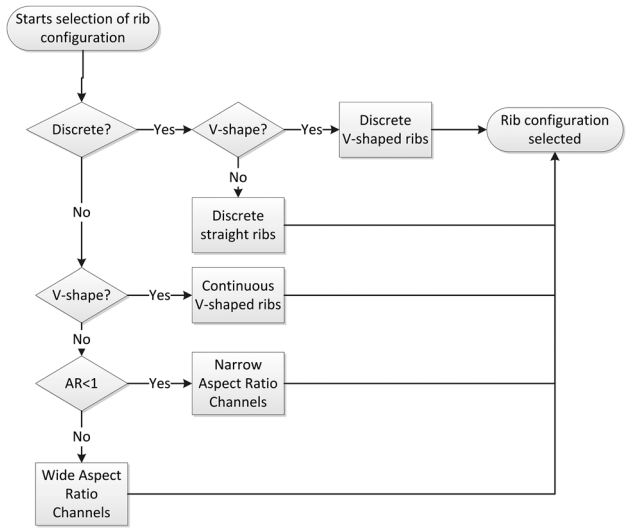

Fig. 5 Flowchart of the turbine cooling

channels (V_m) can be calculated according to the following equation:

$$V_m = \frac{\dot{m}_c}{\rho_c A_{cc}} \tag{15}$$

Then, the Prandtl number Pr and Reynolds number Re inside the channel follow from substitution of the coolant properties and the hydraulic channel diameter (D_h) in Eqs. (16) and (17), respectively,

$$\mathrm{Pr} = \frac{C_{p_c}\mu_c}{\kappa_c} \tag{16}$$

$$\mathrm{Re} = \frac{\rho_c V_m D_h}{\mu_c} \tag{17}$$

What follows is the calculation of the average Stanton number $\overline{S}_t$ to find the heat transfer coefficient h_i, and the average friction factor $\overline{f}$ for the determination of the induced pressure loss Δp. The calculation of the Stanton number and the friction factor depends on the determination of the heat transfer roughness function $G(e^+, Pr)$ and the friction roughness function $R(e^+)$, which rely on the rib configuration and the channel size. Because of the complexity of this multiparameter-dependent heat transfer problem, no direct relation or equation is known to calculate the Stanton number and friction factor and instead semi-empirical correlations are used. The calculation scheme employed for the determination of $\overline{S}_t$ and $\overline{f}$ for the various rib configurations is taken from the literature as presented in Table 1.

Table 1 Calculation scheme references

Rib configuration	Calculation scheme
Discrete V-shaped ribs	Han and Zhang [3]
Discrete straight ribs	Lau et al. [4,5]
Continuous V-shaped ribs	Lau et al. [6]
Narrow aspect ratio channels	Han et al. [7]
Wide aspect ratio channels	Han and Park [8]

After the average Stanton number $\overline{S}_t$ is calculated using one of the calculation schemes, the Nusselt number can be derived using the below equation:

$$\mathrm{Nu} = \overline{S}_t \cdot \mathrm{Re} \cdot \mathrm{Pr} \tag{18}$$

From the Nusselt number, the internal convective heat transfer coefficient can be determined with the following equation, where D_h is the hydraulic diameter:

$$h_i = \frac{\kappa_c \cdot \mathrm{Nu}}{D_h} \tag{19}$$

Using this heat transfer coefficient h_i and the vane/blade geometry data, the overall thermal resistance (R_{in}) from the external metal surface to the coolant slowly inside the cooling channel can be calculated using Eq. (20), where $(L/k)_m$ is the thermal insulance of superalloy metal in $\mathrm{m^2K/W}$, and t_m is the superalloy thickness in meter

$$R_{\mathrm{in}} = \frac{t_m}{(L/k)_m} + \frac{1}{h_i} \tag{20}$$

Finally, the heat absorbed Q_{abs} by the cooling air in a cooling channel section with the length l_x can be calculated from Eq. (21), where T_c is the temperature of the coolant and P_{cc} is the perimeter of the cooling channel section

$$Q_{\mathrm{abs}} = \frac{l_x P_{\mathrm{cc}}(T_{\max} - T_c)}{R_{\mathrm{in}}} \tag{21}$$

The coolant temperature increases due to the heat transferred from the hot wall. The cooling air temperature after the heat absorption (T_{ac}) is calculated using the equation given below:

$$T_{\mathrm{ac}} = T_c + \frac{Q_{\mathrm{abs}}}{\dot{m}_c c_{p_c}} \tag{22}$$

Using the average friction factor $\overline{f}$ that was determined in the applied calculation scheme, the pressure drop (Δp) in the cooling channel section and hence the pressure after cooling p_{ac} is calculated using Eqs. (23) and (24), respectively,

$$\Delta p = \frac{p_c \cdot V_m^2 \cdot l_x \cdot \overline{f}}{2D_h} \tag{23}$$

$$p_{ac} = p_c - \Delta p \tag{24}$$

3.2.2 Pin-Fin Cooling. The cooling mechanism whereby cooling air flowing through a channel is partly blocked by obstacles protruding the channel wall into the free-stream is called pin-fin cooling. Pin-fin cooling is mostly applied in areas where rib turbulated and jet impingement cooling cannot be applied due to manufacturing constraints, like in the trailing edge. In pin-fin cooling, multiple factors affect the heat transfer. First, due to the pins protruding the wall, the channel wall area available for convection cooling is reduced. This reduction is accounted for by the additional area from the pins themselves. Furthermore, the

pin-fins disturb the boundary layer that forms over the wall thereby enhancing the heat transfer.

The Nusselt number calculation of pin-fin cooling follows the calculation scheme and the correlations provided in Ref. [9]. The friction factor correlations presented in Ref. [10] are used to determine the pressure loss caused by the pin-fin array.

The number of pins in spanwise (n_{p_x}) and streamwise (n_{p_y}) direction is calculated by substituting the array width (W_{pf}) and the length (L_{pf}), the pin spacing in spanwise (s/D_p) and streamwise (x/D_p) and the pin diameter D_p in Eqs. (25) and (26), respectively,

$$n_{p_x} = \frac{W_{pf}}{D_{pf} \cdot s/D_{pf}} \tag{25}$$

$$n_{p_y} = \frac{L_{pf}}{D_{pf} \cdot x/D_{pf}} \tag{26}$$

Together with the height of the pin-fin array (and thus the pins) H_p, the free-flow sectional area (A_{ff}) and the heat transfer (i.e., surface exposure) area (A_s) can be calculated by the following equations, respectively,

$$A_{ff} = W_{pf}H_{pf} - (n_{p_x}H_{pf}D_{pf}) \tag{27}$$

$$A_s = W_{pf}H_{pf} + \left[\pi D_{pf} n_{p_x} n_{p_y}\left(H_{pf} - \frac{D_{pf}}{4}\right)\right] \tag{28}$$

Accordingly, the mass flow rate per unit area (G_{pf}) in the array can be calculated using the following equation:

$$G_{pf} = \frac{\dot{m}_c}{A_{ff}} \tag{29}$$

From this mass flow, the Reynolds number Re is calculated using the below equation:

$$\mathrm{Re} = \frac{G_{pf}D_{pf}}{\mu_{\mathrm{air}}} \tag{30}$$

The correlation for N_u as stated in Ref. [9] can now be applied as in Eq. (31). This Nusselt number correlation for staggered pin-fin arrays has been validated for $10^3 < \mathrm{Re} < 10^5$ and $1.5 \leq x/D_{pf} \leq 5$ at given $H_{pf}/D_{pf} = 1$ and $s/D_{pf} = 2.5$. However, after comparison with the data from Refs. [11] and [12], the validity of the correlation can be assumed for $0.5 < H_{pf}/D_{pf} < 3.0$.

$$\mathrm{Nu} = 0.135\,\mathrm{Re}^{0.685}(x/D_{pf})^{-0.34} \tag{31}$$

From this Nusselt number, the heat transfer coefficient h_i and subsequently the total thermal resistance R_{in} from the external metal surface to the coolant in the pin-fin array can be calculated using Eqs. (32) and (33), respectively,

$$h_i = \frac{k_{\mathrm{air}}N_u}{D_{pf}} \tag{32}$$

$$R_{in} = \frac{t_m}{(L/k)_m} + \frac{1}{h_i} \tag{33}$$

Now, the amount of heat absorbed Q_{abs} by the coolant in the pin-fin array can be calculated using Eq. (34), where T_{max} is the maximum AMOT. To account for the heating up of the coolant while it goes through the pin-fin array, the coolant temperature before cooling T_c and after cooling T_{ac} are averaged

$$Q_{\mathrm{abs}} = \frac{A_s\left(T_{\mathrm{max}} - \dfrac{T_c + T_{\mathrm{ac}}}{2}\right)}{R_{\mathrm{in}}} \tag{34}$$

Since the cooling air temperature after cooling is unknown at the beginning, it is assumed to be equal to the cooling air temperature before cooling. For this condition, the absorbed heat Q_{abs} is calculated. Following from the absorbed heat, the coolant temperature after cooling can be calculated using the following equation:

$$T_{\mathrm{ac}} = T_c + \frac{Q_{\mathrm{abs}}}{\dot{m}_c c_{p_{\mathrm{air}}}} \tag{35}$$

This newly found T_{ac} can be used in Eq. (34) for a more accurate heat absorption calculation. This process is repeated until the difference in coolant temperature after cooling T_{ac} between two iterations becomes $T_{\mathrm{ac}} < 10^{-3}$.

As already explained, for calculating the pressure loss, the correlations presented in Ref. [10] are used, in which a different friction factor f correlation depending on the Reynolds number Re has been used. For $10^3 < \mathrm{Re} < 10^4$, Eq, (36) is applied, and for $10^4 < \mathrm{Re} < 10^5$ Eq. (37) is considered

$$f = 0.317\,\mathrm{Re}^{-0.132} \tag{36}$$

$$f = 1.76\,\mathrm{Re}^{-0.138} \tag{37}$$

To determine the pressure loss, the frontal velocity in the pin-fin array (v) needs to be calculated. This is done using Eq. (38) by substituting the density ρ_c and the previously calculated mass flow rate per unit area G_{pf}

$$v = \frac{G_{pf}}{\rho_c} \tag{38}$$

Using calculated v and the friction factor f, the pressure drop Δp in the pin-fin array and subsequently the pressure after cooling p_{ac} can be calculated using the following equations:

$$\Delta p = \frac{1}{2}\rho_c v^2 n_{p_y} f \tag{39}$$

$$p_{\mathrm{ac}} = p_c - \Delta p \tag{40}$$

3.2.3 Jet Impingement Cooling. Jet impingement cooling is a cooling mechanism in which cooling air is pushed through small holes (nozzles) at high velocities and impinges on a hot surface, thereby resulting in high heat transfer coefficient (see Fig. 6). Jet impingement is only applied in areas being exposed to very high thermal loads and thereby requiring high heat transfer coefficient. Jet impingement cooling is therefore mainly applied to the leading edge of rotor blades and vanes.

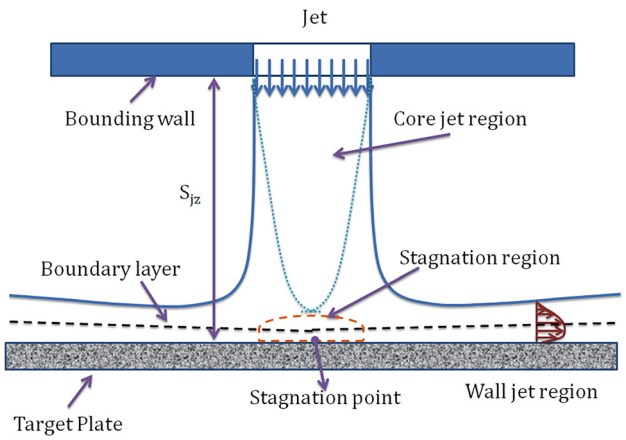

Fig. 6 Schematic of jet impingement

For the jet impingement cooling, various heat transfer correlations from the literature have been studied. For instance, in Ref. [13], the authors deal with the jet impingement arrays where the jets impinge on a flat surface, while, Ref. [14] takes the radius of curvature of the target plate into account. The calculations in Ref. [15] are used for the determination of the pressure loss occurred due to the jet impingement cooling.

The mass flow rate per jet $\dot{m}_j$ is calculated by dividing the total cooling mass flow $\dot{m}_c$ by the number of jets n_j as in the below equation:

$$\dot{m}_j = \frac{\dot{m}_c}{n_j} \tag{41}$$

From the cooling air temperature, the density ρ_c and the Prandtl number Pr can be calculated using Eqs. (42) and (43), respectively,

$$\rho_c = \frac{p_c}{RT_c} \tag{42}$$

$$\mathrm{Pr} = \frac{c_{p_{\mathrm{air}}}\mu_{\mathrm{air}}}{k_{\mathrm{air}}} \tag{43}$$

The impinging jets velocity (V_j) can be calculated using the following equation, where D_j is the jet hole diameter

$$V_j = \frac{4\dot{m}_j}{\rho_c \pi D_j^2} \tag{44}$$

After the jets have impinged on the target surface, the spent cooling air flows away in a direction perpendicular to the impinging jets. This flow is called cross flow, and its velocity V_c can be calculated using Eq. (45), where S_{j_x} is the streamwise hole spacing, and L_{ji} is the length of the jet impingement array. In this simulation, the jet impingement array is assumed to span the entire leading edge of the vane/blade (i.e., $L_{ji} = L_{vb}$)

$$V_c = \frac{\dot{m}_c}{2\rho S_{j_x} L_{ji}} \tag{45}$$

Accordingly, the Reynolds number Re of the jet is obtained from the equation given below:

$$\mathrm{Re} = \frac{\rho_c V_j D_j}{\mu_{\mathrm{air}}} \tag{46}$$

All the parameters required to calculate the average Nusselt number $\overline{\mathrm{Nu}}$ for the jet impingement array are now available. As indicated, two different correlations are used for the calculation of $\overline{\mathrm{Nu}}$.

The Nusselt number correlation for a flat plate from Ref. [13] is presented in Eq. (48). First, several geometry-dependent coefficients have to be calculated. The coefficients A, B, m, and n can be obtained from Eq. (47), for which C, n_x, n_y, and n_z are provided in Table 2. Depending on the arrangements of the jet holes, different coefficients are used. In Table 2, one can notice that the values are given for in line and staggered configurations, respectively,

$$A, m, B, n = C\left(\frac{S_{j_x}}{D_j}\right)^{n_x}\left(\frac{S_{j_y}}{D_j}\right)^{n_y}\left(\frac{S_{j_z}}{D_j}\right)^{n_z} \tag{47}$$

With the coefficients known, the average Nusselt number $\overline{\mathrm{Nu}}$ for a flat plate can be calculated using the equation given below:

$$\overline{\mathrm{Nu}} = A\cdot\mathrm{Re}^m\left(1 - B\left[\left(\frac{S_{j_z}}{D_j}\right)\left(\frac{G_c}{G_j}\right)\right]^n\right)\mathrm{Pr}^{1/3} \tag{48}$$

Table 2 Values of coefficients to be used in Eq. (47) [13]

	Inline pattern				Staggered pattern			
	C	n_x	n_y	n_z	C	n_x	n_y	n_z
A	1.18	−0.944	−0.642	0.169	1.87	−0.771	−0.999	−0.257
m	0.612	0.059	0.032	−0.022	0.571	0.028	0.092	0.039
B	0.437	−0.095	−0.219	0.275	1.03	1.03	−0.307	0.059
n	0.092	−0.005	0.599	1.04	0.442	0.442	−0.003	0.304

In Ref. [14], the average Nusselt number $\overline{\mathrm{Nu}}$ for a jet impingement array of a single row jets are given, and can be found in Eq. (49), where S_{j_z} is the jet-to-target separation distance, D_j is the jet diameter, S_j is the spacing between jet holes, and R_t is the radius of curvature (i.e., diameter) of the target plate. As can be seen from this correlation, the $\overline{\mathrm{Nu}}$ decreases with an increase in the jet-to-target separation distance S_{j_z} and increases with an increase in target surface curvature (i.e., decrease in diameter of the target plate R_t)

$$\overline{\mathrm{Nu}} = 0.63\,\mathrm{Re}^{0.7}\left(\frac{D_j}{S_j}\right)^{0.5}\left(\frac{D_j}{R_t}\right)^{0.6} \times \exp\left[-1.27\left(\frac{S_{j_z}}{D_j}\right)\left(\frac{D_j}{S_j}\right)^{0.5}\left(\frac{D_j}{R_t}\right)^{1.2}\right] \tag{49}$$

With the $\overline{\mathrm{Nu}}$ known, the internal heat transfer coefficient can be calculated using the below equation:

$$h_i = \frac{\overline{\mathrm{Nu}}\cdot k_{\mathrm{air}}}{D_j} \tag{50}$$

Based on this h_i and the vane/blade design data, the total thermal resistance R_{in} from the external metal surface to the coolant in the jet impingement array can be calculated using the following equation:

$$R_{\mathrm{in}} = \frac{t_m}{(L/k)_m} + \frac{1}{h_i} \tag{51}$$

And finally, the heat absorbed Q_{abs} by the jet impinging on the hot target surface can be calculated from Eq. (52), where A_{ji} is the impingement area, and T_c is the temperature of the coolant

$$Q_{\mathrm{abs}} = \frac{A_{ji}(T_{\max} - T_c)}{R_{\mathrm{in}}} \tag{52}$$

The coolant temperature increases due to the heat transfer. The cooling air temperature after the heat absorption T_{ac} is calculated using the following equation:

$$T_{\mathrm{ac}} = T_c + \frac{Q_{\mathrm{abs}}}{\dot{m}_c c_{p_{\mathrm{air}}}} \tag{53}$$

To find the pressure of the coolant after the jet impingement cooling, the pressure loss has to be determined. For this purpose, the correlations in Ref. [15] are used, where two methods for the pressure loss prediction have been discussed. The method used in the turbine cooling module is taken from Ref. [16]. First, the area of the jet A_j and the area of the exit channel A_{ch} are calculated using Eqs. (54) and (55), respectively,

$$A_j = \frac{1}{4}\pi D_j^2 \tag{54}$$

$$A_{\mathrm{ch}} = S_{j_z} L_{ji} \tag{55}$$

Based on these areas, the nozzle inlet resistance coefficient $\xi_{n_{in}}$ and the nozzle friction resistance coefficient $\xi_{n_{fr}}$ can be calculated using Eqs. (56) and (57), respectively, where $t_j = 2.0 \times 10^{-3}$ m is the jet length (i.e., the jet plate thickness)

$$\xi_{n_{in}} = \frac{1}{2}\left(1 - \frac{A_j}{A_{ch}}\right)^{0.75} \tag{56}$$

$$\xi_{n_{fr}} = \frac{64}{\mathrm{Re}}\frac{t_j}{D_j} \tag{57}$$

To calculate the total pressure resistance coefficient ξ_{tot} using Eq. (61), the coefficients C_1, C, and ϕ need to be calculated. Starting with C_1 in Eq. (58), where n_{jx} is the number of nozzles in the streamwise direction

$$C_1 = n_{j_x} \cdot \frac{A_j}{A_{ch}} \tag{58}$$

Substituting C_1 and the previously calculated nozzle inlet resistance $\xi_{n_{in}}$ and nozzle friction resistance coefficient $\xi_{n_{in}}$ in the below equation gives C:

$$C = \frac{C_1}{\sqrt{2 + \xi_{n_{in}} + \xi_{n_{fr}}}} \tag{59}$$

Subsequently, coefficient ϕ can be calculated using Eq. (60). Finally, Eq. (61) is used to find the total pressure resistance coefficient ξ_{tot}

$$\emptyset = 0.09 + 0.5C \tag{60}$$

$$\xi_{tot} = \frac{1}{\tanh \phi^2} - 1 \tag{61}$$

Now using the ξ_{tot}, the exit gas conditions (pressure/temperature/density), the coolant exit velocity V_{out}, and the total pressure loss Δp can be calculated using the following equation:

$$\Delta p = \frac{1}{2}\xi_{tot}\rho_{air}V_{out}^2 \tag{62}$$

Then p_{ac} follows quite logically from the pressure before cooling p_c in the following equation:

$$p_{ac} = p_c - \Delta p \tag{63}$$

3.3 Convergence Scheme. The first four iterations are performed with a very small stepwise increase in the cooling air mass flow from 1×10^{-6} kg/s to 4×10^{-6} kg/s. Following is an exponential fit through these four initial $\dot{m}_c$ points for Q_{in} in the form of $y = ae^{bx}$ and a first-order (i.e., linear) fit for Q_{abs} in the form of $y = ax + b$. In both equations, a and b are the coefficients. These fitted curves are being extrapolated beyond the point where they cross. The point where the lines for Q_{in} and Q_{abs} cross projected on the horizontal axis is the coolant mass flow $\dot{m}_c$ for the next iteration. This step is repeated for the newly found $\dot{m}_c$. When the absorbed heat Q_{abs} and incoming heat Q_{in} at a certain coolant mass flow $\dot{m}_c$ reach within 200 W of each other (i.e., $\Delta Q <= 200$ W), the individual exponential and linear fitting of Q_{abs} and Q_{in} stops and a linearization over ΔQ is applied to find the converged solution.

4 Model Validation

A thorough validation process of the model has been performed in Ref. [17]. The major points of this procedure are explained in this section. A detailed high pressure turbine (HPT) cooling system described in Ref. [18] has been researched under a NASA engine project named energy efficient engine (E^3) as described in Refs. [18] and [19]. This HPT cooling system is used as baseline for verification. A two stages HPT configuration has been considered. The identical turbine geometry parameters in E^3 project are implemented for the cooling model. The values of some essential parameters are provided in Table 3. There are also geometry parameters for different cooling mechanism concerned, which can be found in Ref. [17]. The cooling mass flow rate per vane or per rotor based on the input parameter of Table 3 is provided in Table 4. It can be observed that the simulation data matches very well with the measured data.

Table 3 Parameter values for validation

	NGV	Rotor
Hot gas temperature, T_g (K)	1463	1415
Hot gas pressure, p_g (bar)	23.8	23.5
Coolant temperature, T_c (K)	761	866
Coolant pressure, p_c (bar)	24.5	24.0
Maximal metal temperature, T_{max} (K)	1200	1200
Number of vanes or blades	48	70

Table 4 Cooling mass flow rate per vane or per rotor blade

	NGV		Rotor	
	E^3	Model	E^3	Model
$\dot{m}_c$ (kg/s)	0.021	0.023	0.006	0.004

5 Implementation of the Turbine Cooling Model

In this section, the turbine cooling model is integrated into a gas turbine performance model; accordingly, the parametric analysis is performed by using two cooling methods, i.e., a simplified cooling model used in the literature for preliminary design and a physics-based cooling model based on this paper. Moreover, an engine cycle is optimized by using these two cooling models to quantify the impact of the discrepancy in turbine cooling model on the estimated engine performance.

Following the engine development trend, a very high bypass ratio (BPR) turbofan engine with a geared system representing the state-of-art technology in the year 2025–2030 is proposed as a baseline engine. In Fig. 7, a schematic of such engine architecture is presented with the corresponding station number definitions given in Table 5. The engine performance requirements at various operating conditions are provided in Table 6.

To estimate the engine performance, a zero-D thermodynamic model in accordance with the engine configuration is created using the Gas Turbine Simulation Program (GSP®) [20], which is depicted in Fig. 8. The main gas path of the engine consists of an inlet, fan, low pressure compressor (LPC), high pressure compressor (HPC), combustion chamber, HPT, low pressure turbine (LPT), core convergent nozzle, bypass duct, and convergent bypass nozzle. The bleed control components numbered from 2 to 7 are applied to specify the turbine cooling air requirement as a fraction of the inlet mass flow rate of the HPC ($\dot{m}_c/\dot{m}_{25}$). The requirement of turbine cooling fraction is predicted separately by using the cooling model presented in the earlier section and an empirical model taken from the literature, which will be described later in this section. In the component 0, the thrust requirement is an input. The performance calculation follows the procedure presented in Ref. [21]. The engine off-design performance is derived from the design point performance with the aid of component maps.

The component efficiencies at cruise condition are presented in Table 7. Accordingly, the component efficiencies at other conditions can be derived. The turbine cooling air requirement is

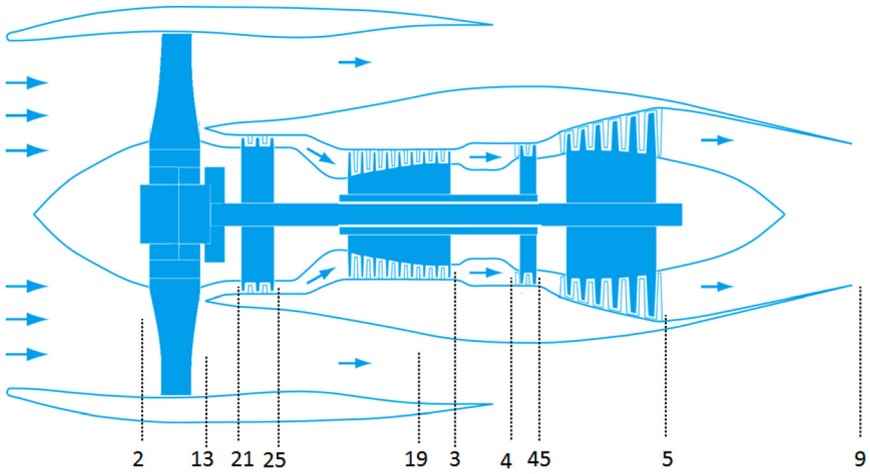

Fig. 7 Schematic of an advanced geared turbofan engine

Table 5 Engine station number definition

Station number	Description
2	Fan inlet
21	Fan core exit
25	LPC exit
3	HPC exit
4	Combustor exit
45	HPT exit
5	LPT exit
9	Core nozzle exit
13	Fan bypass exit
19	Bypass nozzle exit

Table 7 Baseline component performance parameters

Component	Performance parameter	Notation	Datum value	Unit
Fan	Polytropic efficiency	η_{fan}	93	%
LPC	Polytropic efficiency	η_{LPC}	93	%
HPC	Polytropic efficiency	η_{HPC}	91	%
Main combustor	Combustion efficiency	η_{CC}	99.9	%
	Pressure ratio	π_{CC}	0.95	
HPT	Uncooled polytropic efficiency	η_{HPT}	93	%
LPT	Uncooled polytropic efficiency	η_{LPT}	92.5	%
HP shaft	Mechanic efficiency	η_{mHPT}	99.5	%
LP shaft	Mechanic efficiency	η_{mLPT}	99.3	%
Bypass duct	Relative pressure loss	$\Delta p_t/p_{tin}$	2	%

Table 6 Engine performance requirement at various operating conditions

Operating points	Altitude (km)	Mach number	Required thrust (kN)
SLS ISA	0	0	300
Take off	0	0.2	240
Top of climb	11	0.85	60
Cruise	11	0.85	47
Hot-day take off, ISA+15K	0	0	300

predicted at hot-day takeoff, and then is applied to the other operating conditions. The maximum AMOT for the turbine is considered to be 1450 K, which is state of the art and expected to be available in an engine with EIS (entry into service) 2035.

One can notice that in Table 7, the uncooled turbine efficiency has been used. Turbine cooling has a significant effect on the turbine efficiency [22], in the form of bookkeeping [23], or thermodynamic and aerodynamic losses due to the mixing of coolant and hot gas [24]. Quantifying the turbine efficiency losses is not a straightforward process. In the current analysis, a linear correlation has been applied to consider the variation in turbine efficiency attributed due to cooling. The following assumptions have been made:

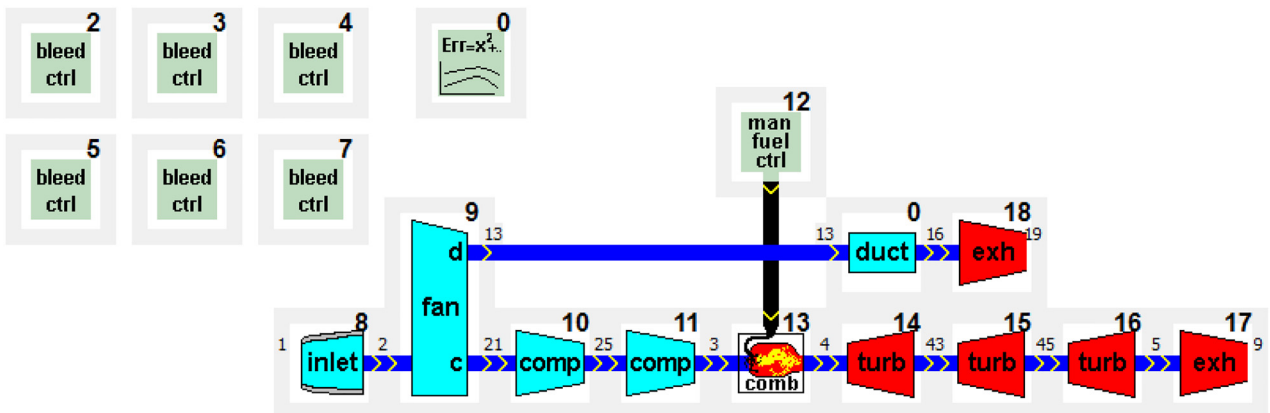

Fig. 8 The layout of a turbofan engine modeled using GSP

Table 8 Basic configurations considered for turbine cooling

Cooling mechanism	Parameter	Symbol	Value	Unit
Rib turbulated cooling	Number of channels	n_{cc}	5/6/3/3	
	Rib height over hydraulic diameter	e/D_h	0.0625	
	Rib pitch over height	P/e	10	
	Rib angle	α_r	60	deg
	Continuous/discrete ribs?	—	Discrete	
	V-shaped/straight ribs?	—	V-shaped	
	Type rib configuration?	—	5	
Pin-fin cooling	Pin diameter	D_p	1.0	mm
	Spanwise spacing	S/D_p	2.5	
	Streamwise spacing	x/D_p	4.0	
	Array width	W_{pf}	15	mm
	Array length	L_{pf}	60	mm
	Pin height	H_p/D_p	1	
	Staggered/inline pattern	—	Staggered	
Jet impingement cooling	Jet impingement area	A_{ji}	2500	mm^2
	Radius of curvature	R_t	20	mm
	Jet diameter	D_j	0.5	mm
	Streamwise jet spacing	S_{jx}	5.0	mm
	Spanwise jet spacing	S_{jy}	5.0	mm
	Jet to target distance	S_{jz}	5.0	mm
	Staggered/inline pattern	—	Staggered	
Film cooling	Film hole diameter	D_f	0.5	mm
	Number of film holes	n_f	60/135/10/60	
	Film holes per row	n_{fr}	15	
	Film hole row spacing	x_r/C_{vb}	0.2	
	Injection angle	α_i	35	deg

- The cooling flow of nozzle guide vane (NGV) completely mixes with the mainstream before its expansion through the blade.
- 50% of the cooling air for the first stage HPT rotor participates in the work output of the turbine rotor.
- The second-stage HPT rotor-cooling air mixes with the mainstream gases after expansion, and therefore, does not contribute to the turbine power output.

5.1 Setup of the Two Cooling Models. The described cooling model is implemented on a turbine blade with a NACA 20424 airfoil. The details about the internal cooling configuration are provided in Table 8. A two-stage turbine configuration is considered, each stage consisting of one stage NGV and one stage rotor. The NACA 20424 airfoil profile has a relative thickness t/c_{vb} of 24% and a camber f/c_{vb} of 20% at location x_f/c_{vb}= 40%. The surface area A_{vb} of the vane/blade is calculated by multiplying its length L_{vb} with its perimeter, P_{vb}.

The size of the cooling channels (in millimeters) in NGV and rotor at each of the turbine stage can be found in Table 9. Since the first stage of the HPT experiences the maximal operating temperature, the most effort has been made to cool this stage. It can be observed that the number of the cooling channels considered in the first stage is nearly twice of the second stage.

Table 9 Size of rib turbulated channels for baseline test engine (in mm)

	NGV1		HPT1		NGV2		HPT2	
#	Width	Height	Width	Height	Width	Height	Width	Height
1	5.0	5.0	1.5	3.0	6.0	6.0	3.0	3.0
2	5.0	10.0	2.5	5.0	6.0	12.0	6.0	6.0
3	8.0	8.0	3.0	6.0	15.0	5.0	6.0	2.0
4	7.5	5.0	5.0	5.0				
5	4.0	2.0	6.0	3.0				
6			3.0	1.0				

In Table 10, the chords and lengths of the vanes/blades, as well as the total amount of vanes/blades per row considered in the modeling, are presented.

For comparison purpose, an empirical correlation for turbine cooling prediction discussed in Ref. [25] is used. The turbine cooling model is represented by the following equation:

$$\frac{\dot{m}_c c_{p,c}}{\dot{m}_g c_{p,g}} = b\left(\frac{T_{g,\text{turbinlet}} - T_b}{T_b - T_{\text{cooling}}}\right)^s \tag{64}$$

In this equation, the coefficients b and s are adjustable, depending on a gas turbine configuration, and T_b is the maximum allowable metal temperature. In the literature [25], it has been suggested that for a single-stage cooled turbine, b should be in the range of 0.05–0.1, depending on the cooling mechanisms (convective or film cooling) and the cooling efficiency, and s is considered to be 1. In this paper, an estimated value for b is considered: $b = 0.06$ (NGV stage), $b = 0.05$ (rotor stage), and $s = 1$. The metal temperature is $T_b = 1450$ K. The specific heat $c_{p,c}$ and $c_{p,g}$ are calculated by the real gas property models. The turbine inlet temperature ($T_{g,\text{turbinlet}}$) and the coolant temperature (T_{cooling}) are taken from the engine performance model.

5.2 Parametric Analysis. The first parametric analysis has been performed for a typical aero engine at International Standard Ambient (ISA) sea level static (SLS) condition. The engine BPR, fan pressure ratio (FPR), low pressure compressor pressure ratio, and the total inlet mass flow rate are kept constant, as provided in

Table 10 Size of a vane/blade and the number of vanes and rotor per stage

Vane/blade	Stage	Chord (mm)	Length (mm)	Amount
NGV vane	1	63	56	80
	2	66	76	144
HPT blade	1	42	62	144
	2	44	93	160

Table 11 Baseline input parameters at SLS ISA condition

Engine parameters	Values
BPR	12
FPR	1.4
LPC PR	3.0
HPC PR	[8.0, 18.0]
HPT IT (K)	[1500, 2000]
Inlet air mass flow rate (kg/s)	1308
Maximum allowable metal turbine metal temperature (K)	1450

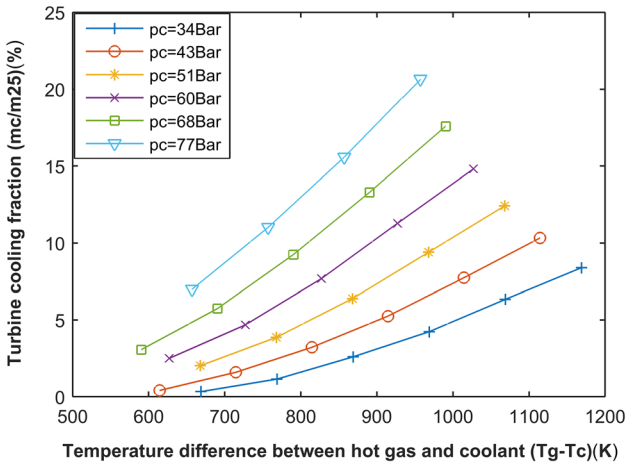

Fig. 9 Variation in turbine cooling fraction versus temperature difference between hot gas and coolant for different coolant pressures. The cooling requirement is predicted by the in-house turbine cooling tool. AMOT = 1450 K.

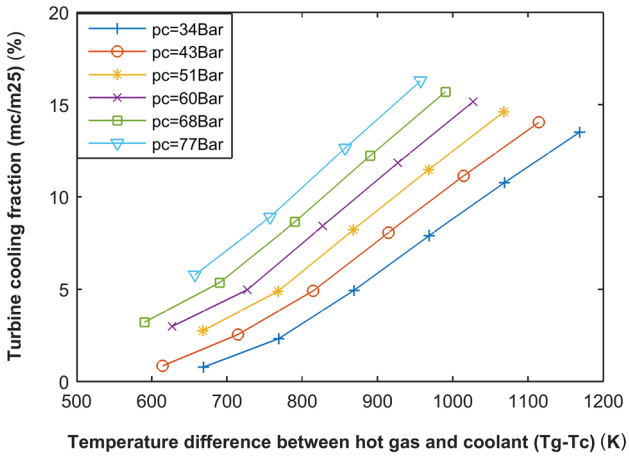

Fig. 10 Variation in turbine cooling fraction versus temperature difference between hot gas and coolant for different coolant pressures. The cooling requirement is predicted by the empirical turbine cooling correlation (Eq. (64)). AMOT = 1450K.

Table 11. For the parametric analysis, varying the HPT inlet temperature is varied from 1500 to 2000 K with a step of 100 K; meanwhile varying the HPC pressure ratio from 8 to 18 in an incremental step of 2. All the component efficiencies remain constant as given in Table 7. The maximal AMOT has been assumed as 1450 K for simulation using both models.

The variation in turbine cooling air fraction ($\dot{m}_c/\dot{m}_{\text{inletHPC}}$) predicted by two cooling models are presented in Figs. 9 and 10. The x axis represents the temperature difference between hot gas and

Table 12 Baseline input parameters at SLS ISA condition

Engine parameters	Values
BPR	12
FPR	1.4
OPR	75.6
HPT IT (K)	[1700,2000]
Inlet air mass flow rate (kg/s)	1308
AMOT (K)	[1250,1550]

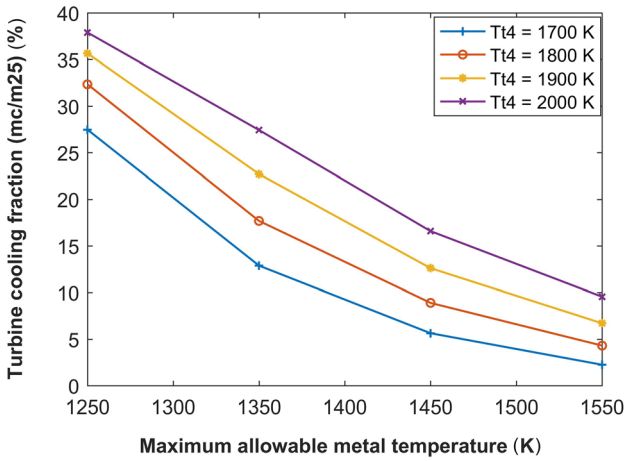

Fig. 11 Variation in turbine cooling fraction versus the AMOT for different TIT. The in-house cooling prediction tool used.

Table 13 The engine design space and optimization constraints at cruise

Bounds of design parameters		Constraints	
FPR	[1.2, 1.8]	OPR	≤70
LPC pressure ratio	[1.4, 5.0]	FN (kN)	=47
HPC pressure ratio	[8, 20]	$\dot{m}_a$ at the engine inlet	Constant
Tt4 (K)	[1400, 1900]		
BPR	[8, 15]		

the coolant, and the changes in coolant pressure (p_c in the figure legend) have been mainly due to the variation of engine OPR.

A general trend can be observed in both figures that as T_g increases, the turbine cooling requirement increases. Moreover, the turbine cooling requirement increases as the coolant pressure increases (due to increase in OPR) for the same temperature difference. On the other hand, one can observe that when the coolant pressure is low, the empirical correlation tends to overestimate the turbine cooling requirement, the maximum difference can be more than double, whereas, as the coolant pressure increases, the discrepancy in turbine cooling flow reduces. When the coolant pressure becomes very high, the empirical model underestimated the turbine cooling air requirement compared to the in-house model. Furthermore, it can be seen that the turbine cooling flow in Fig. 10 increases linearly with respect to the coolant pressure. However, in Fig. 9, the turbine cooling derived by the in-house model increases nonlinearly with coolant pressure. This nonlinearity becomes stronger when the temperature discrepancy between T_g and T_c increases.

The second parametric analysis has been performed using the in-house turbine cooling model, where the coolant temperature, hot gas temperature, and AMOT are varied independently. The analysis intends to give an insight into the effects of these

Table 14 Engine performance at cruise and hot day take off

	SLS ISA + 15K		Cruise	
Parameters	Empirical model	In-house cooling model	Empirical model	In-house cooling model
BPR	14.3	14.6	14.6	14.9
FPR	1.49	1.46	1.5	1.47
OPR	68	67	70	70
HPT inlet temperature (K)	2168	2278	1791	1892
LPT inlet temperature (K)	1451	1436	1178	1168
Inlet air mass flow rate (kg/s)	1122	1159	471	494
HPT cooling fraction (%)	24	34	24	34
LPT cooling fraction (%)	0.1	0	0.1	0
FN (kN)	300	300	47	47
Thrust specific fuel consumption (g/kN/s)	6.8	6.9	13.5	13.8

parameters on the coolant requirement. The variation range of each parameter is given in Table 12.

The variation in turbine cooling fraction with respect to the AMOT and HPT inlet temperature is presented in Fig. 11. It can be seen that the turbine cooling requirement reduces significantly as the AMOT increases from 1250 K to 1550 K. The same trend is valid for different turbine inlet temperature (T_{t4}).

5.3 The Impact of Turbine Cooling on Engine Performance. In this section, the cycle optimization is performed concerning two turbine cooling strategies, namely, the empirical turbine cooling model provided in Eq. (64) and the in-house turbine cooling model. The comparison will be made to evaluate the effects of the turbine cooling on engine performance.

The objective is to minimize the cruise thrust specific fuel consumption. The engine performance requirement is specified in Table 6, and the component efficiencies given in Table 7 are used in this section. The cycle optimization is performed at cruise condition, whereas, the turbine cooling requirement is estimated at the SLS ISA + 15K condition. The MATLAB fmincon optimizer using sequential quadratic programming algorithm is implemented for the cycle optimization [26]. The same design space defined in Table 13 is considered for engine cycle optimization.

Engine performance at cruise and hot-day take off is given in Table 14. It can be seen that using the empirical model, the turbine cooling requirement is underestimated by about 30%. Accordingly, the optimized engine has a lower T_4 and a smaller size. Moreover, the cycle efficiency of the engine using the empirical turbine cooling model is slightly higher than that of the engine using the cooling model in this paper.

6 Conclusions

In the current research, a semi-empirical tool has been developed to evaluate the turbine cooling requirements in the preliminary design stage. The validation of the cooling model has been conducted with the HPT cooling system studied in a previous NASA engine project (E^3). The model is then used to assess the effects of turbine cooling on gas turbine performance.

The main conclusions of this research are:

- Comparison to a baseline cooling system (E^3 cooling) shows that the proposed cooling model works sufficiently well to serve its purpose during an engine conceptual design phase.
- The air required for turbine cooling increase exponentially with an increase in the turbine inlet temperature for a given maximum allowable metal temperature.
- Whereas most of the cooling models in the literature predict a linear increase in turbine cooling air with temperature, the current model proves that the increase is steeper.
- If the nonlinear increase in the cooling air requirement is not modeled correctly, the gas turbine performance can be significantly overestimated.
- The correct estimation of turbine cooling requirement becomes important when operating at high TIT and/or OPR, as the cooling air requirements have a pronounced effect on the gas turbine performance.

Nomenclature

A = area (m^2)
c_p = specific heat (J/kg/K)
c_{vb} = blade/vane cord (m)
D = diameter (m)
D_h = hydraulic diameter (m)
F_N = net thrust (kN)
k = thermal conductivity (W/mK)
l = length (m)
$(L/k)_m$ = thermal resistance (m^2 K/W)
$\dot{m}$ = mass flow rate (kg/s)
Nu = Nusselt number
Pr = Prandtl number
Q = heat (J)
r = recovery factor
Re = Reynolds number
s = spanwise spacing (m)
St = Stanton number
T = temperature (K)
t_m = material thickness (m)
Tu = turbulence intensity
V = velocity (m/s)
x = at a given location (m)
α = injection angle (deg)
μ = dynamic viscosity (N s/m^2)
ρ = density kg/m^3

Subscripts

abs = absorption
ac = after cooling
aw = adiabatic wall
c = cooling
cc = cooling channel
cf = crossflow
f = fuel
ff = free flow
g = gas
h = hot flow
in = input
iw = inside wall
J = jet
pf = pin-fin
max = maximal
x = streamwise direction
y = spanwise direction
3 = exit of high pressure compressor

4 = turbine inlet
23 = exit of low pressure compressor
∞ = free stream

Abbreviations

AMOT = maximal allowable metal temperature (K)
BPR = bypass ratio
HPC = high pressure compressor
HPT = high pressure turbine
ISA = International Standard Ambient
LPC = low pressure compressor
LPT = low pressure turbine
NGV = nozzle guide vane
OPR = overall pressure ratio
PR = pressure ratio
SLS = sea level static
TIT = turbine inlet temperature (K)

References

[1] Yin, F., 2016, "Modeling and Characteristics of a Novel Multi-Fuel Hybrid Engine for Future Aircraft," Doctoral thesis, Delft University of Technology, Delft, The Netherlands.
[2] Baldauf, S. A., Scheurlen, M., Schulz, A., and Wittig, S., 2002, "Correlation of Film Cooling Effectiveness From Thermographic Measurements at Engine Like Conditions," ASME Paper No. GT2002-30180.
[3] Han, J. C., and Zhang, Y. M., 1992, "High Performance Heat Transfer Ducts With Parallel Broken and V-Shaped Broken Ribs," Int. J. Heat Mass Transfer, **35**(2), pp. 513–523.
[4] Lau, S. C., McMillin, R. D., and Han, J. C., 1991, "Heat Transfer Characteristics of Turbulent Flow in a Square Channel With Angled Discrete Ribs," ASME J. Turbomach., **113**(3), pp. 367–374.
[5] Lau, S. C., McMillin, R. D., and Han, J. C., 1991, "Turbulent Heat Transfer and Friction in a Square Channel With Discrete Rib Turbulators," ASME J. Turbomach., **113**(3), pp. 360–366.
[6] Lau, S. C., Kukreja, R. T., and McMillin, R. D., 1991, "Effects of V-Shaped Rib Arrays on Turbulent Heat Transfer and Friction of Fully Developed Flow in a Square Channel," Int. J. Heat Mass Transfer, **34**(7), pp. 1605–1616.
[7] Han, J. C., Ou, S., Park, J. S., and Lei, C. K., 1989, "Augmented Heat Transfer in Rectangular Channels of Narrow Aspect Ratios With Rib Turbulators," Int. J. Heat Mass Transfer, **32**(9), pp. 1619–1630.
[8] Han, J. C., and Park, J. S., 1988, "Developing Heat Transfer in Rectangular Channels With Rib Turbulators," Int. J. Heat Mass Transfer, **31**(1), pp. 183–195.
[9] Metzger, D., Shepard, W., and Haley, S., 1986, "Row Resolved Heat Transfer Variations in Pin-Fin Arrays Including Effects of Non-Uniform Arrays and Flow Convergence," ASME Paper No. 86-GT-132.
[10] Metzger, D., Fan, Z., and Shepard, W., 1982, "Pressure Loss and Heat Transfer Through Multiple Rows of Short Pin Fins," Seventh International Conference, Munich, Germany, Sept. 6–10.
[11] VanFossen, G. J., 1982, "Heat-Transfer Coefficients for Staggered Arrays of Short Pin Fins," ASME J. Eng. Power, **104**(2), pp. 268–274.
[12] Arora, S. C., and Abdel Messeh, W., 1983, "Heat Transfer Experiments in High Aspect Ratio Rectangular Channel With Epoxied Short Pin Fins," ASME Paper No. 83-GT-57.
[13] Florschuetz, L., Truman, C., and Metzger, D., 1981, "Streamwise Flow and Heat Transfer Distributions for Jet Array Impingement With Crossflow," ASME J. Heat Transfer, **103**(2), pp. 337–342.
[14] Chupp, R. E., Helms, H. E., and McFadden, P. W., 1969, "Evaluation of Internal Heat-Transfer Coefficients for Impingement-Cooled Turbine Airfoils," J. Aircr., **6**(3), pp. 203–208.
[15] Levy, Y., Rao, A. G., Erenburg, V., Sherbaum, V., Gaissinski, I., and Krapp, V., 2012, "Pressure Losses for Jet Array Impingement With Crossflow," ASME Paper No. GT2012-68386.
[16] Idel′chik, I. E., and Steinberg, M. O., 1996, *Handbook of Hydraulic Resistance*, Begell House, New York.
[17] Tiemstra, F., 2014, "Design of a Semi-Empirical Tool for the Evaluation of Turbine Cooling Requirements in a Preliminary Design Stage," Master's thesis, Delft University of Technology, Delft, The Netherlands.
[18] Halila, E. E., Lenahan, D. T., and Thomas, T. T., 1982, "Energy Efficient Engine High Pressure Turbine Test Hardware Detailed Design Report," National Aeronautics and Space Administration, Cleveland, OH, Technical Report No. NASA CR-167955.
[19] Stearns, E. M., 1982, "Energy Efficient Engine Core Design and Performance Report," National Aeronautics and Space Administration, Cincinnati, OH, Technical Report No. NASA-CR-168069.
[20] Visser, W. P., and Broomhead, M. J., 2000, "GSP, a Generic Object-Oriented Gas Turbine Simulation Environment," ASME Paper No. 2000-GT-0002.
[21] Saravanamuttoo, H. I. H., Rogers, G. F. C., Cohen, H., and Straznicky, P. V., 2008, *Gas Turbine Theory*, 6th ed, Pearson Education Ltd., Harlow, UK.
[22] Hartsel, J., 1972, "Prediction of Effects of Mass-Transfer Cooling on the Blade-Row Efficiency of Turbine Airfoils," Tenth Aerospace Sciences Meeting, San Diego, CA, pp. 1–7.
[23] Kurzke, J., 2002, "Performance Modeling Methodology: Efficiency Definitions for Cooled Single and Multistage Turbines," ASME Paper No. GT2002-30497.
[24] Young, J., and Horlock, J., 2006, "Defining the Efficiency of a Cooled Turbine," ASME J. Turbomach., **128**(4), pp. 658–667.
[25] Jonsson, M., Bolland, O., Bücker, D., and Rost, M., 2005, "Gas Turbine Cooling Model for Evaluation of Novel Cycles," International ECOS Conference, Trondheim, Norway, June 20–22, pp. 641–650.
[26] MathWorks, 2015, "MATLAB Support Documentation—Optimization Toolbox Function," The MathWorks Inc., Natick, MA, accessed Apr. 4, 2018, http://nl.mathworks.com/help/optim/ug/fmincon.html